Fronts of spin tunneling in molecular magnets

D. A. Garanin
Department of Physics, Lehman College, City University of New York, 250 Bedford Park Boulevard West, Bronx, New York 10468-1589, USA

(Received 29 April 2009; revised manuscript received 14 June 2009; published 2 July 2009)

Dissipative spin-tunneling transitions at biased resonances in molecular magnets such as Mn_{12} Ac are controlled by the dipolar field that can bring the system on and off resonance. It is shown that this leads to spin relaxation in form of propagating fronts of tunneling, with the dipolar field adjusting self-consistently to provide a zero bias within the front core. There are two regimes of the front propagation: laminar and nonlaminar with discontinuous magnetization and dipolar field. In the laminar regime the speed of the front can exceed that of the magnetic deflagration, if the transverse field is large enough. Fronts of tunneling can be initiated by magnetic field sweep near the end of the crystal.

DOI: 10.1103/PhysRevB.80.014406 PACS number(s): 75.50.Xx, 75.45.+j, 76.20.+q

I. INTRODUCTION

Molecular magnets (MM), including their first and mostly studied representative Mn_{12} Ac,[1] have initially attracted attention as molecules with the effective big spin $S=10$ showing bistability as a result of a strong uniaxial anisotropy $-DS_z^2$.[2] Resonance spin tunneling manifested in the magnetic hysteresis loops[3–5] with steps at the field-values $B \approx B_k = kD/(g\mu_B)$, $k=0, \pm 1, \pm 2, \ldots$ made molecular magnets a hotspot of research during more than 10 years.

Crystals of molecular magnets do not show a significant exchange interaction because the magnetic core of the molecule is screened by organic ligands. Thus, magnetic molecules remain largely superparamagnetic, although MM can order below 1 K due to dipole-dipole interactions (DDI).[6,7]

An important role of the DDI is that the dipolar field created by the spins is large enough to change the resonance condition for the up and down spins and thus to strongly influence spin tunneling. Fully ordered spins in an elongated Mn_{12} Ac crystal create the dipolar-field $B^{(D)} \simeq 52.6$ mT at a molecule.[7,8] This becomes comparable with the resonance width defined by the tunnel splitting Δ in transverse magnetic fields above 5 T, for the $k=1$ tunneling resonance. For smaller transverse fields, Δ is much smaller and thus the DDI can completely block the resonant tunneling. The action of the dipolar field is dynamical and self-consistent since tunneling of spins causes the dipolar field to change, blocking or allowing resonant transitions.

The role of the DDI in spin tunneling was recognized in Refs. 9–16 where Monte Carlo simulations were done on the basis of a phenomenological model involving discrete jumps of the spins through the instantaneous "tunneling window." The main purpose of these studies was to explain the $\sqrt{t}$ relaxation experimentally observed in Mn_{12} Ac.[17]

It was not understood until recently that DDI in molecular magnets can result in spatially inhomogeneous states creating the dipolar field such that the system is on resonance in some regions of space where spins can relax, leading to moving fronts. An example is the domain wall in elongated dipolar-ordered crystals of Mn_{12} Ac at low temperatures. The reduced dipolar field at $T=0$ in Fig. 2 of Ref. 7 is close to zero in the region around the center of the domain wall with the width on the order of the crystal's thickness. It should be mentioned that Mn_{12} Ac remains the only molecular magnet that can be grown in long crystals required for such kind of phenomena.

Similar effects can take place in the tunneling at biased resonances, $k \geq 1$. If the external field approaches the resonance by a slow sweep, as was the case in many experiments, moving walls of tunneling can be created near the ends of long crystals (where the dipolar bias is smaller) and then penetrate into their depth with a speed unrelated to the sweep rate.[18] The role of the sweep is only to create an initial state for the wall of tunneling to start. It was argued that this mechanism can explain the width of the steps in dynamic hysteresis curves[3–5] by the time needed for the wall of tunneling to cross the crystal. Nonuniformity of the magnetization in Mn_{12} Ac developing during spin tunneling was detected by local measurements earlier.[19]

The walls or self-organized patterns of spin tunneling investigated in Ref. 18 are not exactly fronts because they are lacking the combined space-time dependence on the argument $z-vt$ only, where v is the speed of the front. Frozen-in quasiperiodic spatial structures have been found behind these moving walls. In fact, true smooth fronts of spin tunneling do exist in the range of the external bias smaller than that in Ref. 18. Studying these fronts and their transition to the moving walls with a nonuniformity behind with increasing the bias is the purpose of this article. It will be shown that there are two regimes.

For the external bias not exceeding a critical value, the true fronts (that can be called "laminar") are realized in which the dipolar field adjusts to create a resonance in the front region. In the limit of strong dipolar field (relative to the resonance width) the front speed and the magnetization behind the front can be calculated analytically and are independent of the strength of the DDI.

For a larger external bias, the magnetization distribution and thus the dipolar field in the wall cannot fully adjust to provide the resonance condition. In this case the wall is moving with a quasiperiodically varying speed leaving a quasiperiodic state behind. The average wall speed decreases with the DDI strength quadratically.

The dipolar mechanism of spin tunneling is resembling magnetic deflagration in Mn_{12} Ac.[20,21] Here, instead of the

 ©2009 The American Physical Society

temperature, the relaxation rate is controlled by the self-consistent dipolar field bringing the system on or off resonance. Thus, in a sense, one can call the phenomenon studied here *cold deflagration*. Of course, the heat release in the course of the cold deflagration can give rise to the regular deflagration, especially for high resonances k and well thermally isolated crystals. In this case the two kinds of deflagration can compete.

The rest of the article is organized as follows: in Sec. II the dynamics of spin tunneling between the metastable ground state and a resonant excited state on the other side of the barrier is considered. The simplified overdamped equations of motion are obtained in the case of the tunnel-splitting frequency $\Delta/\hbar$ smaller than the damping of the excited state $\Gamma_{m'}$. It is further argued that in the presence of disorder that spreads resonances one can use overdamped equations in a generalized form also for larger Δ. In Sec. III the dipolar field created by a wall of magnetization is calculated for the cylindrical and ribbon geometries. In Sec. IV the full system of cold-deflagration equations is written and transformed into dimensionless form. In Sec. V the limit of strong DDI is studied and analytical expressions for the residual magnetization behind the front and the front speed are obtained. Section VI provides the results of numerical calculations in both regimes of the wall propagation.

II. SPIN TUNNELING AND RELAXATION

We will be using the generic giant-spin model of molecular magnets with the Hamiltonian

$$\hat{H} = -DS_z^2 - g\mu_B B_z S_z - g\mu_B B_x S_x + \ldots, \tag{1}$$

where D is the uniaxial anisotropy and

$$\mathbf{B} = \mathbf{B}_{\text{ext}} + \mathbf{B}^{(D)} \tag{2}$$

is the total magnetic field, including the external and dipolar fields. Suppressed terms in the Hamiltonian can include the biaxial and fourth-order anisotropy that can make a contribution into the tunnel-splitting Δ of the resonant spin up and down states. Since the most interesting situation arises in the case of a large Δ that can only be created by a strong transverse field, the dropped terms will not be needed. For $B_x=0$ the exact quantum states of $\hat{H}$ are $|m\rangle$ with $-S \le m \le S$, their energies being $\varepsilon_m = -Dm^2 - g\mu_B B_z m$. The resonance-condition $\varepsilon_m = \varepsilon_{m'}$ between *all* states $|m\rangle$ on the left side of the barrier $(m<0)$ and $|m'\rangle$ on the right side of the barrier $(m'=-m-k)$ is satisfied for the resonance-fields

$$B_z = B_k, \quad B_k = kD/(g\mu_B), \quad k = 0,1,\ldots \tag{3}$$

This resonance condition turns out to be independent of the transverse field.

Application of the transverse field leads to the two effects. First, each state $|m\rangle$ hybridizes with neighboring states within the same well forming the state that can be denoted as $|\psi_m\rangle$. Physically, this corresponds to spin canting in the direction of the transverse field. Second, the states $|\psi_m\rangle$ on different sides of the barrier hybridize because of the resonance spin tunneling near $B_z = B_k$. Of course, one can speak of the states $|\psi_m\rangle$ for not-too-strong transverse field, so that there still are low-lying states well localized within one of the wells. The states $|\psi_m\rangle$ provide a basis for a simplified treatment of spin tunneling and relaxation near resonances that otherwise has to be considered within the density-matrix formalism.[22,23]

Consider the metastable ground state of a molecular magnet, $|\psi_m\rangle = |\psi_{-S}\rangle$, near a tunneling resonance with an excited-state $|\psi_{m'}\rangle$ on the right side of the barrier, Fig. 1 of Ref. 18. The dynamics of tunneling at low temperatures is described by the subset of the density-matrix equation (DME) taking into account only these two levels. The level $|\psi_{m'}\rangle$ can decay into lower-lying levels within the same well with rate $\Gamma_{m'}$. Since there are no incoming relaxation processes for the state $|\psi_{m'}\rangle$ at low temperatures, the DME can be simplified to the form of the damped Schrödinger equation

$$\dot{c}_{-S} = -\frac{i}{2}\frac{\Delta}{\hbar} c_{m'}$$

$$\dot{c}_{m'} = \left(\frac{iW}{\hbar} - \frac{1}{2}\Gamma_{m'}\right) c_{m'} - \frac{i}{2}\frac{\Delta}{\hbar} c_{-S}. \tag{4}$$

Here, Δ is the tunnel splitting and $W \equiv \varepsilon_m - \varepsilon_{m'}$ is the energy bias between the two levels,

$$W = (S+m')g\mu_B(B_z - B_k + B_z^{(D)}) \equiv W_{\text{ext}} + W^{(D)}. \tag{5}$$

In fact, here one should use the values of S and m' corrected for spin canting. Since $|\psi_{-S}\rangle$ is the lowest state in the left well, it cannot decay. The numbers of particles in the states are defined by

$$n_{-S} = |c_{-S}|^2, \quad n_{m'} = |c_{m'}|^2, \tag{6}$$

etc. The spin polarization in our low-temperature tunneling process is given by $\langle S_z\rangle = -Sn_{-S} + \Sigma_{m=m'}^{S} mn_m$. As the states with $m = m'+1, \ldots, S-1$ decay faster than $|\psi_{m'}\rangle$, their contribution can be neglected. Then for the normalized spin-average variable

$$\sigma_z \equiv \langle S_z\rangle/S, \tag{7}$$

one obtains

$$\sigma_z = 1 - 2n_{-S} - (1 - m'/S)n_{m'}. \tag{8}$$

In the overdamped case $\Gamma_{m'} \gg \Delta/\hbar$ the variable $c_{m'}$ in Eq. (4) adiabatically adjusts to the instantaneous value of c_{-S}. Setting $\dot{c}_{m'} = 0$ in the second of these equations one obtains

$$c_{m'} = \frac{\Delta}{2\hbar}\frac{c_{-S}}{W/\hbar + i\Gamma_{m'}/2}. \tag{9}$$

Inserting it into the first of Eq. (4) one obtains

$$\dot{c}_{-S} = -\frac{i\Delta^2}{4\hbar^2}\frac{c_{-S}}{W/\hbar + i\Gamma_{m'}/2}. \tag{10}$$

With the help of Eq. (6), one obtains the equation for the metastable population n_{-S} in the form

$$\dot{n} = -\Gamma n, \tag{11}$$

where the subscript $-S$ has been dropped for transparency and the dissipative tunneling rate Γ is given by[22]

$$\Gamma = \frac{\Delta^2}{2\hbar^2}\frac{\Gamma_{m'}/2}{(W/\hbar)^2 + (\Gamma_{m'}/2)^2}. \tag{12}$$

In the overdamped limit one has $n_{m'} \ll n_{-S} \equiv n$, so that Eq. (8) simplifies to

$$\sigma_z = 1 - 2n. \tag{13}$$

The decay-rate $\Gamma_{m'}$ is mainly due to the relaxation between the adjacent energy levels in the right well, $\Gamma_{m'} = \Gamma_{m',m'+1}$, see Eq. (A9) of Ref. 24 or Eq. (294) of Ref. 23. For $k=1$ and thus $m'=9$ one has $\Gamma_{m'} \approx 10^7$ s^{-1}, while $\Delta/\hbar$ reaches a comparable value in the transverse field above 3 T. At higher transverse fields the tunneling dynamics should be underdamped. Resonances with higher k have larger splitting Δ and become underdamped in smaller transverse fields.

In the case of underdamped resonances, $\Delta/\hbar \gtrsim \Gamma_{m'}$, the rate of dissipative spin tunneling can be described by the integral relaxation time $\tau_{\rm int}$ resulting in the effective rate[23]

$$\Gamma = \frac{1}{\tau_{\rm int}} = \frac{\Delta^2}{2\hbar^2}\frac{\Gamma_{m'}/2}{\Omega^2 + (\Gamma_{m'}/2)^2}, \tag{14}$$

where

$$(\hbar\Omega)^2 \equiv W^2 + \frac{1}{4}\left(1 + \frac{S-m'}{2S}\right)\Delta^2. \tag{15}$$

One can see that in the underdamped case the width of the Lorentzian becomes of the order of $(\Delta/2)/\hbar$, compared to $\Gamma_{m'}/2$ in the overdamped case. Although Eq. (11) with Γ given by Eq. (14) does not accurately describe the oscillating dynamics of the system in the underdamped case, in particular the Landau-Zener effect, it will be used below as an approximation for the many-body problem with coupling via the dipolar field in both overdamped and underdamped cases. A more rigorous approach based on Eq. (4) requires much more computer time because of fast oscillations. On the other hand, oscillations at tunneling resonances have never been experimentally observed in MM because of the resonance spread as a result of ligand disorder and other factors. For the low-bias resonances such as $k=1$ and thus $m'=S-1$ the contribution of $n_{m'}$ in Eq. (8) can be neglected, thus Eq. (13) will be used in all cases.

III. DIPOLAR FIELD

The dipolar field and ensuing dipolar bias of tunneling resonances in crystals of molecular magnets have been discussed in details in Ref. 7, so that only a short summary with necessary changes will be provided below.

The z component of dipolar field at site i (i.e., at a particular magnetic molecule), created by molecular spins polarized along the z axis is given by

$$B_{i,z}^{(D)} = \frac{Sg\mu_B}{v_0} D_{i,zz}, \quad D_{i,zz} \equiv \sum_j \phi_{ij}\sigma_{jz}, \tag{16}$$

where v_0 is the unit-cell volume and

$$\phi_{ij} = v_0 \frac{3(\mathbf{e}_z \cdot \mathbf{n}_{ij})^2 - 1}{r_{ij}^3}, \quad \mathbf{n}_{ij} \equiv \frac{\mathbf{r}_{ij}}{r_{ij}}. \tag{17}$$

Inside a uniformly magnetized ellipsoid the dipolar field is uniform and one has $D_{zz} = \bar{D}_{zz}\sigma_z$, where

$$\bar{D}_{zz} = \bar{D}_{zz}^{(\rm sph)} + 4\pi\nu(1/3 - n^{(z)}), \tag{18}$$

ν is the number of magnetic molecules per unit cell and $n^{(z)}=0$, 1/3, and 1 for a cylinder, sphere, and disk, respectively. $\bar{D}_{zz}^{(\rm sph)}$ depends on the lattice structure. For Mn_{12} Ac lattice summation yields $\bar{D}_{zz}^{(\rm sph)}=2.155$ that results in $\bar{D}_{zz}^{(\rm cyl)}=10.53$ for a cylinder. Then Eq. (16) yields the dipolar field $B_z^{(D)} \simeq 52.6$ mT in an elongated sample that was also obtained experimentally.[8]

The dipolar bias $W^{(D)}$ in Eq. (5) can be written in the form

$$W^{(D)} = \left(1 + \frac{m'}{S}\right) E_D D_{zz}, \tag{19}$$

where

$$E_D \equiv (Sg\mu_B)^2/v_0 \tag{20}$$

is the dipolar energy, $E_D/k_B = 0.0671$ K for Mn_{12} Ac. Since the dipolar field depends on the magnetization and its values in an elongated crystal can change between -52.6 and 52.6 mT, one can conclude that, according to Eq. (5), the resonance condition $W=0$ can be, in principle, satisfied in the dipolar tunneling window around the resonance -52.6 mT $\le B_z - B_k \le 52.6$ mT. This dipolar window is much smaller than the distance between the two tunneling resonances that is about 0.5 T. Practically, for a negative external bias $B_z - B_k$ the relaxation is hindered by the causality: to produce a positive dipolar field that would balance the negative external bias, spins should already be on the right side of the barrier.

For a cylinder of length L and radius R with the symmetry axis z along the easy axis, magnetized with $\sigma_z = \sigma_z(z)$, the reduced z field along the symmetry axis has the form

$$D_{zz}(z) = \int_{-L/2}^{L/2} dz' \frac{2\pi\nu R^2 \sigma_z(z')}{[(z'-z)^2 + R^2]^{3/2}} - k\sigma_z(z), \tag{21}$$

where

$$k \equiv 8\pi\nu/3 - \bar{D}_{zz}^{(\rm sph)} = 4\pi\nu - \bar{D}_{zz}^{(\rm cyl)} > 0, \tag{22}$$

$k=14.6$ for Mn_{12} Ac. In particular, for a long uniformly polarized cylinder one obtains

$$D_{zz}(z) = \frac{2\pi\nu z}{\sqrt{z^2 + R^2}}\sigma_z + (\bar{D}_{zz}^{(\rm sph)} - 2\pi\nu/3)\sigma_z. \tag{23}$$

At the left end of the long cylinder, $z=0$, one has $D_{zz} = (\bar{D}_{zz}^{(\rm sph)} - 2\pi\nu/3)\sigma_z$. For Mn_{12} Ac one obtains $D_{zz} = -2.03\sigma_z$, having the sign opposite to that of the field in the depth,

$\bar{D}_{zz}^{(\mathrm{cyl})}\sigma_z$. This means that a homogeneously magnetized state in the resonance external field $B_z=B_k$ may be unstable with respect to spin tunneling beginning in the vicinity of the ends of the cylinder, as at some point near the end the resonance condition $D_{zz}(z)=0$ is satisfied. To the contrary, dipolar field in the depth of a uniformly magnetized cylinder provides the dipolar bias that puts the system off resonance and makes the transition rate Γ very small. If the external field B_z is swept in the positive direction toward the resonance, spin tunneling begins near the ends of the crystal and then it propagates inside the crystal as a moving wall of tunneling, as the dipolar field changes self-consistently.[18]

One can also calculate the dipolar field on the z symmetry axis of a slab of length L and sides a and b. In the case $a \sim b$ the results are similar to those for the cylinder above. For a thick slab (a ribbon) with $a \ll b$ one obtains

$$D_{zz}(z) = \int_{-L/2}^{L/2} dz' \frac{2a\nu\sigma_z(z')}{(z'-z)^2+(a/2)^2} - k\sigma_z(z) \tag{24}$$

that has the kernel less localized than that of Eq. (21).

IV. COLD-DEFLAGRATION EQUATIONS

The phenomenon of cold deflagration is described by a collection of Eq. (11) for every magnetic molecule in the crystal, with the dipolar field controlling transitions being determined by the instantaneous nonuniform magnetization. As the full three-dimensional (3D) problem with a long-range interaction requires too much computer power, here the one-dimensional approximation will be made. The magnetization is considered as a function of the coordinate z only, i.e., the deflagration fronts are flat, and the dipolar field is taken along the symmetry axis as in Eq. (21) that will be used below. Of course, the dipolar field away from the symmetry axis is different, that will result in nonflat fronts. However, to avoid complications in demonstrating the basic phenomenon, these effects will be ignored here.

It is convenient to introduce the dimensionless time $\tilde{t}$ and coordinate $\tilde{z}$ as

$$\tilde{t} \equiv \Gamma_{\mathrm{res}} t, \quad \tilde{z} \equiv z/R, \tag{25}$$

where Γ_{res} is the resonance relaxation rate following from Eq. (14) with $(S-m')/(2S)$ neglected,

$$\Gamma_{\mathrm{res}} = \frac{\Delta^2}{\hbar^2} \frac{\Gamma_{m'}}{(\Delta/\hbar)^2+\Gamma_{m'}^2}. \tag{26}$$

Then Eq. (11) becomes

$$\frac{d}{d\tilde{t}} n(\tilde{z},\tilde{t}) = -F(\tilde{z},\tilde{t}) n(\tilde{z},\tilde{t}), \tag{27}$$

where F contains integral dependence on $n(\tilde{z},\tilde{t})$ via $D_{zz}(\tilde{z},\tilde{t})$,

$$F(\tilde{z},\tilde{t}) = \frac{1}{1+4\tilde{E}_D^2 \tilde{W}^2(\tilde{z},\tilde{t})}, \quad \tilde{E}_D \equiv \frac{2E_D}{\sqrt{\Delta^2+\hbar^2\Gamma_{m'}^2}}. \tag{28}$$

The dimensionless bias $\tilde{W}=W/(2E_D)$, with W defined by Eq. (5), has the form

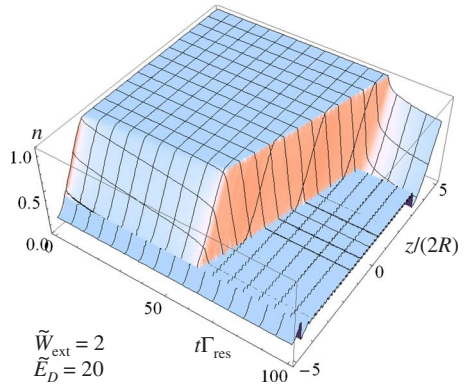

FIG. 1. (Color online) Propagating front of cold deflagration for $\tilde{W}_{\mathrm{ext}}=2$ and $\tilde{E}_D=20$. Cold deflagration starts after some ignition time that depends on the initial condition.

$$\tilde{W}(\tilde{z},\tilde{t}) = \tilde{W}_{\mathrm{ext}} + \tilde{W}^{(D)}(\tilde{z},\tilde{t}) = \tilde{W}_{\mathrm{ext}} + D_{zz}(\tilde{z},\tilde{t}), \tag{29}$$

where

$$\tilde{W}_{\mathrm{ext}} = \frac{Sg\mu_B}{E_D}(B_z - B_k) \tag{30}$$

and $D_{zz}(\tilde{z},\tilde{t})$ defined by Eq. (21) can be rewritten in the form

$$D_{zz}(\tilde{z},\tilde{t}) = \int_{-\tilde{L}/2}^{\tilde{L}/2} d\tilde{z}' \frac{2\pi\nu\sigma_z(\tilde{z}',\tilde{t})}{[(\tilde{z}'-\tilde{z})^2+1]^{3/2}} - k\sigma_z(\tilde{z},\tilde{t}), \tag{31}$$

where $\sigma_z(\tilde{z},\tilde{t})=1-2n_{-S}(\tilde{z},\tilde{t})$ and $\tilde{L} \equiv L/R$.

For a long sample, $\tilde{L}\to\infty$, one can seek for a solution of Eq. (27) in the form of a moving front depending on the combined argument $\xi \equiv z-vt$, where v is the front speed. In reduced units one has $\tilde{\xi} \equiv \tilde{z}-v^*\tilde{t}$, where the relation between the real and reduced front speeds has the form

$$v = v^* \Gamma_{\mathrm{res}} R. \tag{32}$$

Equation (27) for the front becomes

$$v^* \frac{dn}{d\tilde{\xi}} = F(\tilde{\xi}) n, \tag{33}$$

where $F(\tilde{\xi})=[1+4\tilde{E}_D^2\tilde{W}^2(\tilde{\xi})]^{-1}$ contains

$$D_{zz}(\tilde{\xi}) = \int_{-\infty}^{\infty} d\tilde{\xi}' \frac{2\pi\nu\sigma_z(\tilde{\xi}')}{[(\tilde{\xi}'-\tilde{\xi})^2+1]^{3/2}} - k\sigma_z(\tilde{\xi}). \tag{34}$$

Equation (32) makes the dependence of v on R and Γ_{res} obvious. However, there are nontrivial parameters $\tilde{E}_D$ and $\tilde{W}_{\mathrm{ext}}$ that enter v^*.

For a ribbon one can introduce $\tilde{z} \equiv 2z/a$ and replace Eqs. (31) and (34) by the corresponding expressions following from Eq. (24).

The cold-deflagration equations can be solved by discretization that reduces them to a system of nonlinear ordinary first-order differential equations. The front of tunneling for $\tilde{E}_D=20$ and $\tilde{W}_{\mathrm{ext}}=2$ is shown in Figs. 1 and 2 while more details will be given in Secs. VI and VII.

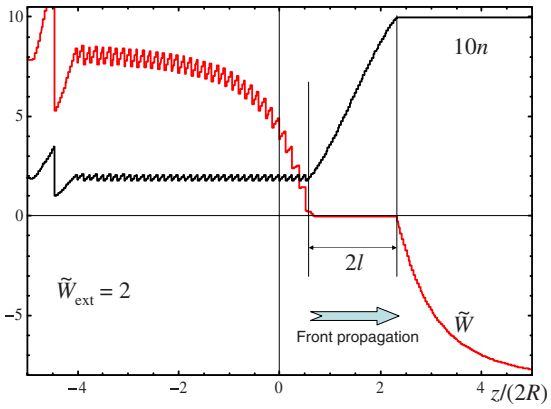

FIG. 2. (Color online) Spatial profiles of the metastable population n and the reduced bias $\tilde{W}$ in the front for $\tilde{W}_{ext}=2$ and $\tilde{E}_D=20$. Everywhere in the front the system is near the resonance, $\tilde{W}\approx 0$. At this value of the bias periodic structures behind the front begin to emerge.

V. LIMIT OF STRONG DIPOLAR FIELD

Unless a strong transverse field is applied, the numerical value of $\tilde{E}_D$ of Eq. (28) for Mn_{12} Ac is large. In particular, in the overdamped limit $\tilde{E}_D \cong E_D/(\hbar\Gamma_{m'}) \approx 10^3$ for $m'=S-1$. In this case one could think that F is negligibly small everywhere except for a very close vicinity of the resonance, so that the total relaxation and thus the speed of the front are very small. However, as the numerical solution shows, the system finds the way to relax faster by forming a front region of a width $l \sim R$ where $\tilde{W}$ is small and F is of order one. In this extended region resonant tunneling transitions take place. Beyond the front region $\tilde{W}$ deviates from zero and F becomes negligibly small. As a result, $n(\xi)$ changes practically only within the front core.

Basing on these insights, one can construct a perturbative expansion in powers of $1/\tilde{E}_D$ and show that the solution $n(\tilde{\xi})$ and the front speed v^* become independent of $\tilde{E}_D$ for $\tilde{E}_D \gg 1$. One can search for $\sigma_z(\tilde{\xi})$ in the form

$$\sigma_z(\tilde{\xi}) \cong \sigma_z^{(0)}(\tilde{\xi}) + \sigma_z^{(1)}(\tilde{\xi})/\tilde{E}_D, \tag{35}$$

and similarly for $n(\tilde{\xi})=[1-\sigma_z(\tilde{\xi})]/2$. The term $\sigma_z^{(0)}(\tilde{\xi})$ is defined by the condition that within the front region $-\tilde{l} \le \tilde{\xi} \le \tilde{l}$, with the width $\tilde{l}$ to be determined self-consistently, the contribution of $\sigma_z^{(0)}(\tilde{\xi})$ into the bias $\tilde{W}$ is zero. If this is fulfilled, the term $4\tilde{E}_D^2\tilde{W}^2$ in the denominator of Eq. (28) is of order one due to the correction $\sigma_z^{(1)}(\tilde{\xi})$, so that in the front-region F is of order one. In the region before the front, $\tilde{l} < \tilde{\xi}$, one has $n^{(0)}(\tilde{\xi})=1$ and $\sigma_z^{(0)}(\tilde{\xi})=\sigma_{zi}=-1$. Everywhere behind the front, $\tilde{\xi} < -\tilde{l}$, one has final values $n^{(0)}(\tilde{\xi})=n_f$ and $\sigma_z^{(0)}(\tilde{\xi})=\sigma_{zf}$ that are to be determined. In the front region the condition $\tilde{W}=0$ with Eq. (29) yields the integral equation

$$\tilde{W}^{(0)}(\tilde{\xi}) = 0, \quad -\tilde{l} \le \tilde{\xi} \le \tilde{l}, \tag{36}$$

where

$$\tilde{W}^{(0)}(\tilde{\xi}) = \tilde{W}_{ext} + \int_{-\tilde{l}}^{\tilde{l}} d\tilde{\xi}' \frac{2\pi\nu\sigma_z^{(0)}(\tilde{\xi}')}{[(\tilde{\xi}'-\tilde{\xi})^2+1]^{3/2}} - k\sigma_z^{(0)}(\tilde{\xi}) + 2\pi\nu\left[\sigma_{zi}\left(1+\frac{\tilde{\xi}-\tilde{l}}{\sqrt{(\tilde{\xi}-\tilde{l})^2+1^2}}\right) + \sigma_{zf}\left(1-\frac{\tilde{\xi}+\tilde{l}}{\sqrt{(\tilde{\xi}+\tilde{l})^2+1^2}}\right)\right]. \tag{37}$$

This equation determines the zero-order profile $\sigma_z^{(0)}(\tilde{\xi})$, including $\tilde{l}$ and σ_{zf}.

Equation (36) can be solved numerically by discretizing the integral using $N+1$ equidistant points within the interval $(-\tilde{l},\tilde{l})$ given by $\tilde{\xi}_i=-\tilde{l}+2\tilde{l}i/N$, $i=0,1,\ldots,N$. The value at the right end of the interval is fixed by the boundary-condition $\sigma_z^{(0)}(\tilde{\xi}_N)=\sigma_{zi}=-1$. Thus, there are total $N+1$ unknowns including $\tilde{l}$, that can be found by solving the system of $N+1$ equations $\tilde{W}^{(0)}(\tilde{\xi}_i)=0$ with $i=0,1,\ldots,N$. Note that this system of equations is nonlinear because of $\tilde{l}$. In this way one finds the zero-order magnetization profile in the front and the magnetization behind the front σ_{zf} for any $\tilde{W}_{ext}>0$. In particular, for Mn_{12} Ac one obtains $\tilde{l}=0.848$.

On the other hand, one can find important analytical results if one searches for the solution in the form

$$\sigma_z^{(0)}(\tilde{\xi}) = \frac{\sigma_{zf}+\sigma_{zi}}{2} - \frac{\sigma_{zf}-\sigma_{zi}}{2} f(\tilde{\xi}), \tag{38}$$

where $f(\pm\tilde{l})=\pm 1$. Substituting this into Eq. (37) one obtains the equation for $f(\tilde{\xi})$

$$0 = \tilde{W}_{ext} - \frac{\sigma_{zf}-\sigma_{zi}}{2}\int_{-\tilde{l}}^{\tilde{l}} d\tilde{\xi}' \frac{2\pi\nu f(\tilde{\xi}')}{[(\tilde{\xi}'-\tilde{\xi})^2+1]^{3/2}} + k\frac{\sigma_{zf}-\sigma_{zi}}{2} f(\tilde{\xi}) + \bar{D}_{zz}^{(cyl)}\frac{\sigma_{zf}+\sigma_{zi}}{2} - \pi\nu(\sigma_{zf}-\sigma_{zi}) \times\left(\frac{\tilde{\xi}+\tilde{l}}{\sqrt{(\tilde{\xi}+\tilde{l})^2+1^2}} + \frac{\tilde{\xi}-\tilde{l}}{\sqrt{(\tilde{\xi}-\tilde{l})^2+1^2}}\right), \tag{39}$$

where $\bar{D}_{zz}^{(cyl)}=4\pi\nu-k$. One can see that there are even and odd terms in $\tilde{\xi}$ in this equation and $f(\tilde{\xi})$ is odd. The even and odd parts of this equation should turn to zero independently of each other. For the even part one obtains the equation

$$0 = \tilde{W}_{ext} + \bar{D}_{zz}^{(cyl)}\frac{\sigma_{zf}+\sigma_{zi}}{2} \tag{40}$$

that with $\sigma_{zi}=-1$ yields $\sigma_{zf}=1-2\tilde{W}_{ext}/\bar{D}_{zz}^{(cyl)}$ and

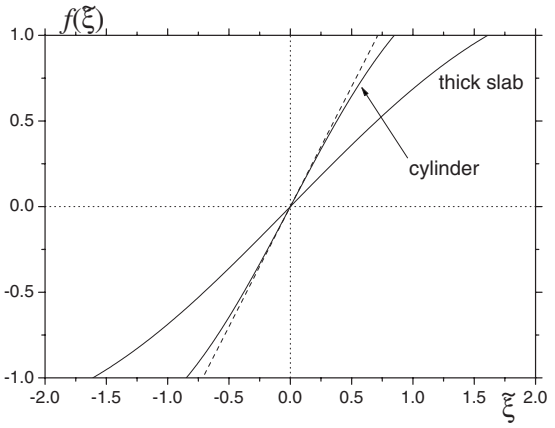

FIG. 3. Normalized magnetization profile in the cold-deflagration front for long Mn_{12} Ac crystals of cylindrical and thick-slab shape. Approximate result for the cylinder is shown by a dashed line.

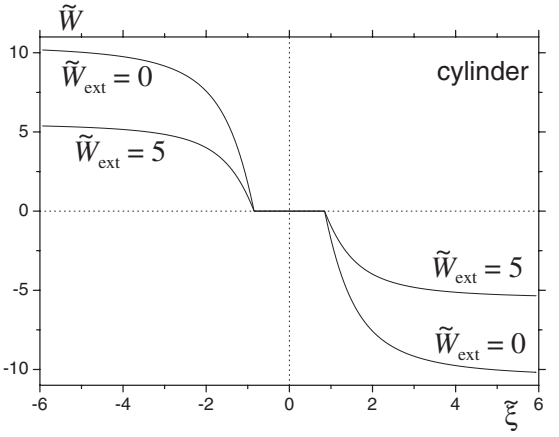

FIG. 4. Normalized energy bias $\tilde{W}$ in the cold-deflagration front in long Mn_{12} Ac crystals in the limit of strong dipolar field. In the central part of the front $\tilde{W} \cong 0$ so that resonance transitions take place.

$$n_f = \frac{1-\sigma_{zf}}{2} = \frac{\tilde{W}_{\rm ext}}{\bar{D}_{zz}^{(\rm cyl)}} \tag{41}$$

for the fraction of metastable molecules behind the front. Note that since $0 \le n_f \le 1$, this solution only exists for

$$0 \le \tilde{W}_{\rm ext} \le \bar{D}_{zz}^{(\rm cyl)}. \tag{42}$$

The odd part of Eq. (39) yields the equation

$$-\int_{-\tilde{l}}^{\tilde{l}} d\tilde{\xi}' \frac{f(\tilde{\xi}')}{[(\tilde{\xi}'-\tilde{\xi})^2+1]^{3/2}} + \frac{k}{2\pi\nu} f(\tilde{\xi}) = \frac{\tilde{\xi}+\tilde{l}}{\sqrt{(\tilde{\xi}+\tilde{l})^2+1^2}} + \frac{\tilde{\xi}-\tilde{l}}{\sqrt{(\tilde{\xi}-\tilde{l})^2+1^2}} \tag{43}$$

that defines $f(\tilde{\xi})$ and $\tilde{l}$. They can be found numerically by discretization as described above. The expression for $n^{(0)}(\tilde{\xi})$ in terms of $f(\tilde{\xi})$ following from Eq. (38) has the form

$$n^{(0)}(\tilde{\xi}) = \frac{1}{2}\left(1 + \frac{\tilde{W}_{\rm ext}}{\bar{D}_{zz}^{(\rm cyl)}}\right) + \frac{1}{2}\left(1 - \frac{\tilde{W}_{\rm ext}}{\bar{D}_{zz}^{(\rm cyl)}}\right) f(\tilde{\xi}). \tag{44}$$

Using the method of Ref. 7, one can show that the approximate solution for $f(\tilde{\xi})$ valid for $|\tilde{\xi}| \ll 1$ has the form

$$f_{\rm app}(\tilde{\xi}) = \tilde{\xi}/\tilde{l}_{\rm app}, \tag{45}$$

where

$$\tilde{l}_{\rm app} = \frac{k}{\sqrt{(4\pi\nu)^2 - k^2}}. \tag{46}$$

For a Mn_{12} Ac cylinder one obtains $\tilde{l}_{\rm app} = 0.7137$.

Numerically found $f(\tilde{\xi})$ and its approximation $f_{\rm app}(\tilde{\xi})$ for a Mn_{12} Ac cylinder is shown in Fig. 3 together with $f(\tilde{\xi})$ for a thick slab (ribbon) discussed at the end of this section. In Fig. 4, the reduced energy bias $\tilde{W}$ is shown in the cylindric geometry for different values of the external bias.

The speed of the front v^* can be found by considering the effect of the correction $\sigma_z^{(1)}(\tilde{\xi})$, although one does not need to evaluate this correction explicitly. In Eq. (33) one has to keep $\sigma_z^{(1)}(\tilde{\xi})$ in F. This makes F zero order in $1/\tilde{E}_D$. On the other hand, $dn/d\tilde{\xi}$ and n outside F can be taken at zero order in $1/\tilde{E}_D$. One thus can rewrite Eq. (33) in the interval $-\tilde{l} < \tilde{\xi} < \tilde{l}$ in the form

$$\frac{v^*}{F} = g(\tilde{\xi}), \quad g(\tilde{\xi}) \equiv n^{(0)} \left(\frac{dn^{(0)}}{d\tilde{\xi}}\right)^{-1}. \tag{47}$$

There is a point inside the interval $-\tilde{l} < \tilde{\xi} < \tilde{l}$ where W changes its sign. At this point $1/F$ reaches its minimal value 1. On the other hand, this point can be determined as the minimum of the right-hand side of this equation. Then, obviously,

$$v^* = \min[g(\tilde{\xi})]. \tag{48}$$

Using Eq. (44) one obtains

$$g(\tilde{\xi}) = \frac{Q + 1 + f(\tilde{\xi})}{f'(\tilde{\xi})}, \quad Q \equiv \frac{2\tilde{W}_{\rm ext}}{\bar{D}_{zz}^{(\rm cyl)} - \tilde{W}_{\rm ext}}. \tag{49}$$

One can see that for $\tilde{W}_{\rm ext} = 0$ one has $\min[g(\tilde{\xi})] = 0$, achieved at $\tilde{\xi} = \tilde{l}$ where $f = -1$. This yields $v^* = 0$ at $\tilde{W}_{\rm ext} = 0$. In the general case one has to investigate

$$g'(\tilde{\xi}) = 1 - \frac{f''(\tilde{\xi})}{f'^2(\tilde{\xi})}[Q + 1 + f(\tilde{\xi})]. \tag{50}$$

Since $g'(-\tilde{l}) = 0$ at

$$Q = Q_c = f'^2(-\tilde{l})/f''(-\tilde{l}), \tag{51}$$

one concludes that for $Q \le Q_c$ the minimum is achieved at $\tilde{\xi} = -\tilde{l}$ and thus

$$v^* = \frac{Q}{f'(-\tilde{l})} = \frac{\tilde{W}_{\rm ext}}{\bar{D}_{zz}^{(\rm cyl)} - \tilde{W}_{\rm ext} f'(-\tilde{l})} \frac{2}{}. \tag{52}$$

For a cylinder of Mn_{12} Ac one has $2/f'(-\tilde{l})=2.31$ and $Q_c=0.809$. According to Eq. (49), the latter translates into $\tilde{W}_{{\rm ext},c}=3.03$. Then Eq. (30) yields the value of the corresponding bias-field $B_{z,c}-B_k=15$ mT. For $B_k \le B_z \le B_{z,c}$, the front speed in real units obtained with the help of Eqs. (30), (16), and (20) is given by

$$v = R\Gamma_{\rm res} \frac{B_z - B_k}{B_z^{(D)} - B_z + B_k f'(-\tilde{l})} \frac{2}{}. \tag{53}$$

For $Q_c \le Q$ (and thus $\tilde{W}_{{\rm ext},c} \le \tilde{W}_{\rm ext}$) one has to find $\min[g(\tilde{\xi})]$ from the condition $g'(\tilde{\xi})=0$ that leads to somewhat smaller front speeds than given by the formulas above. However, the laminar regime of the cold-deflagration fronts breaks down at the external bias smaller than $\tilde{W}_{{\rm ext},c}$, so that the results of this section for $\tilde{W}_{{\rm ext},c} \le \tilde{W}_{\rm ext}$ are irrelevant.

Let us now consider the slab geometry. From Eq. (24) with $\tilde{z} \equiv 2z/a$ instead of Eq. (37) one obtains the equation

$$\tilde{W}^{(0)}(\tilde{\xi}) = \tilde{W}_{\rm ext} + \int_{-\tilde{l}}^{\tilde{l}} d\tilde{\xi}' \frac{4\nu\sigma_z^{(0)}(\tilde{\xi}')}{(\tilde{\xi}' - \tilde{\xi})^2 + 1} - k\sigma_z^{(0)}(\tilde{\xi}) + 4\nu\left[\sigma_{zi}\left(\frac{\pi}{2} + \mathrm{Arctan}(\tilde{\xi} - \tilde{l})\right) + \sigma_{zf}\left(\frac{\pi}{2} - \mathrm{Arctan}(\tilde{\xi} + \tilde{l})\right)\right]. \tag{54}$$

The numerically obtained result for the normalized magnetization profile $f(\tilde{\xi})$ is shown of Fig. 3, compared to that of a cylinder. Since the kernel in the integral equation for the slab is less localized for a thick slab than for a cylinder, the front-width $\tilde{l}=1.61$ for a thick slab is larger than $\tilde{l}=0.848$ for the cylinder. All formulas obtained above are valid for a thick slab as well, however with different constants: $2/f'(-\tilde{l})=4.79$, $Q_c=0.540$, and $\tilde{W}_{{\rm ext},c}=2.24$.

VI. NUMERICAL RESULTS

As mentioned at the end of Sec. IV, the cold-deflagration equations can be solved by discretization reducing them to a system of ordinary differential equation. Numerical calculations use the semi-infinite geometry including the region of length $-L/2 \le z \le L/2$ where equations are solved plus the range $L/2 < z \le \infty$ where the magnetization is fixed to $\sigma_z=-1$ corresponding to the metastable state. The latter is needed to create the dipolar field in the main region $-L/2 \le z \le L/2$ that corresponds to the semi-infinite sample. This allows to operate on shorter samples that saves computer time. When the deflagration front reaches $z=L/2$, it cannot go further, so the results near this point become unphysical and should be ignored.

The first thing revealed by computations is that for large values of $\tilde{E}_D$ it is very important to prepare the system in the initial state close to the actual front, with $\tilde{W} \approx 0$ within the front core. The further is the initial state from this optimal state, the more time (ignition time) the system needs to adjust so the front could start moving across the sample. For initial states far from the front states, the ignition time can be so long that there is a significant off-resonance relaxation in the bulk of the crystal during it. For smaller dipolar fields such as $\tilde{E}_D \sim 3$ (that can be achieved by applying a strong transverse field to increase Δ), ignition of the fronts is much easier. Another possibility to ignite the cold deflagration is to slowly sweep the external field in the positive direction, approaching the resonance,[18] which will be considered later on.

Computations for large $\tilde{E}_D$ and not-too-strong bias $\tilde{W}_{\rm ext}$ corroborate semianalytical results of the preceding section. For z not too close to the ends of the interval $-L/2 \le z \le L/2$, the variables indeed depend on $\xi=z-vt$, as it should be in a moving front. 3D plots of $n(z,t)$ are smooth and look qualitatively as in Fig. 1, and the ignition time can be reduced to zero by a better choice if the initial state. The metastable population $\bar{n}(t)$ averaged over the length of the crystal is almost flat during the ignition time, then it decreases linearly as the front travels through the crystal, then becomes nearly flat again after the front arrives at the right end of the interval $-L/2 \le z \le L/2$, see Fig. 16 of Ref. 21 for the standard magnetic deflagration and Fig. 4 of Ref. 18 for the cold deflagration. The front speed can be obtained as $v = L/(t_{\rm arrival} - t_{\rm ignition})$.

The reduced front speed v^*, Eq. (32), vs $\tilde{W}_{\rm ext}$, Eq. (30), is shown for $\tilde{E}_D=100$ in Fig. 5(a). For not-too-large bias, $\tilde{W}_{\rm ext} \lesssim 1$, the numerical results are in good agreement with Eq. (52) shown by a solid line. In this region the numerical results do not depend on the number of discrete points used in the solution. Similar results for $\tilde{E}_D=20$ in Fig. 5(b) are further from the theoretical curve (not shown) because the condition of a strong dipolar field is not fully satisfied. Also there is some nonzero speed in the region $\tilde{W}_{\rm ext} < 0$ that is, however, quickly decreasing with the negative bias.

With increasing the external bias, the laminar solution in the form of a smooth moving front loses its stability. In Fig. 2 one can already see wiggles behind the front that represent frozen-in spatial structures with the period of order R. With increasing $\tilde{W}_{\rm ext}$ or $\tilde{E}_D$, these features progress and the region of transitions moves with oscillating speed (see Fig. 6). To distinguish this transition region from the true front, it was called "wall of transitions."[18] It would cost significant additional efforts to find out analytically or numerically whether the transition from the laminar to nonlaminar regime with increasing $\tilde{W}_{\rm ext}$ is gradual or there is a threshold. One important observation is that the spatial structures behind the front are discontinuous on z, while the analytical result of Eq. (48) was obtained based on the assumption that the solution is continuous.

As the laminar regime breaks down, the instability is manifested by the dependence of the results for v^* in Fig. 5 on the number of discretization points. With increasing N the discontinuities in $v^*(\tilde{W}_{\rm ext})$ become smaller but, unfortunately, increasing N is limited by computing resources. For larger

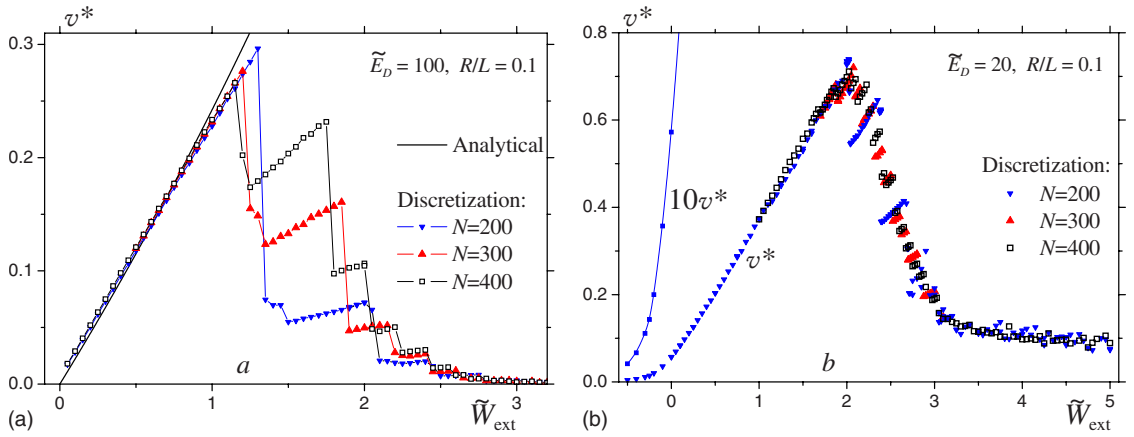

FIG. 5. (Color online) Reduced front-speed v^* vs the reduced bias $\widetilde{W}_{\rm ext}$ for different discretizations. In (a) for $\widetilde{E}_D=100$ and $\widetilde{W}_{\rm ext}\lesssim 1$ the numerical results are in a good accordance with Eq. (52) (straight line).

$\widetilde{W}_{\rm ext}$ the front speed reaches a plateau that depends on $\widetilde{E}_D$, and curves with different discretizations converge again.

In the nonlaminar regime the magnetization in the front cannot completely adjust so that bias in the front core would be very close to zero and the resonance transitions could occur at a rate close to the maximal rate $\Gamma_{\rm res}$. This is the reason why $v^*(\widetilde{W}_{\rm ext})$ drops after reaching a maximum, as the instability begins. Still the very existence of the front in this case suggests that the system is closer to the resonance in this region than in the others. The values of $\widetilde{W}$ in the front should be of order 1, so that in Eq. (28) one has $F\sim 1/\widetilde{E}_D^2$. This is supported by the computations shown in Fig. 7: in the plateau region (in particular for $\widetilde{W}_{\rm ext}=5$) the front speed fits to

$$v^* \simeq 8/\widetilde{E}_D^2 \tag{55}$$

for large $\widetilde{E}_D$.

VII. COLD DEFLAGRATION INITIATED BY FIELD SWEEP

As was mentioned above, for most of initial conditions the development of the cold-deflagration front requires a very long ignition time. If the initial condition is chosen in a special way close to the actual front, the process starts immediately. However, one cannot find a practical way to prepare such initial state.

Fortunately, as was found in Ref. 18, the front can be ignited by a slow time-linear sweep $W_{\rm ext}=v_W t$ starting with a value of $W_{\rm ext}$ that ensures $W<0$ everywhere in the sample (see Fig. 8). The sweep rate can be conveniently parametrized by $\varepsilon\equiv\pi\Delta^2/(2\hbar v_W)$ and slow sweep requires $\varepsilon\gg 1$. As $W_{\rm ext}$ increases, the condition $W=0$ would be first reached at the end of the sample, then the resonance point would move into its depth. However, transitions induced by the sweep (seen in Fig. 8 before the ignition) change the dipolar field so that the system does not cross the resonance in the region near the end of the sample, although it becomes close to the resonance in the increasingly broad region (see Fig. 9). The reason for this is that flipping spins in a small region near the end of the sample do not significantly change the dipolar field from the surface of the crystal, the integral term of Eq. (21), but strongly change the local contribution, last term in this formula. Increasing σ_z due to resonance transitions leads to the *decrease* in the local term that creates a negative dipolar bias and prevents the system from crossing

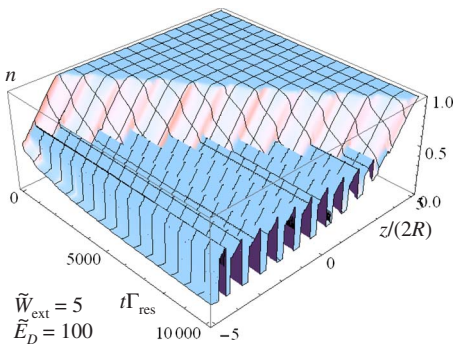

FIG. 6. (Color online) Propagating front of cold deflagration for $\widetilde{E}_D=100$ and $\widetilde{W}_{\rm ext}=5$. Here ignition time was eliminated by a good choice of the initial condition. The front speed is oscillating and there are spatially periodic structures behind the front.

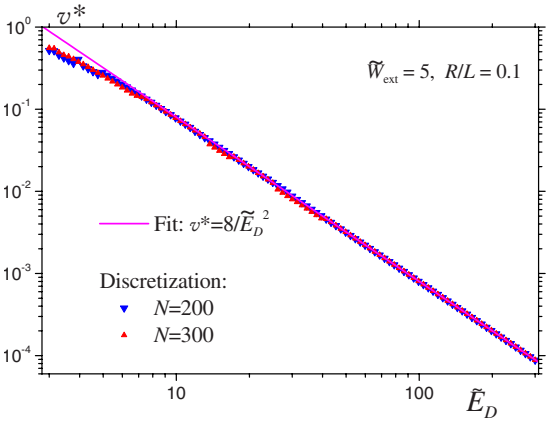

FIG. 7. (Color online) Front-speed v^* vs $\widetilde{E}_D$ in the nonlaminar regime for $\widetilde{W}_{\rm ext}=5$.

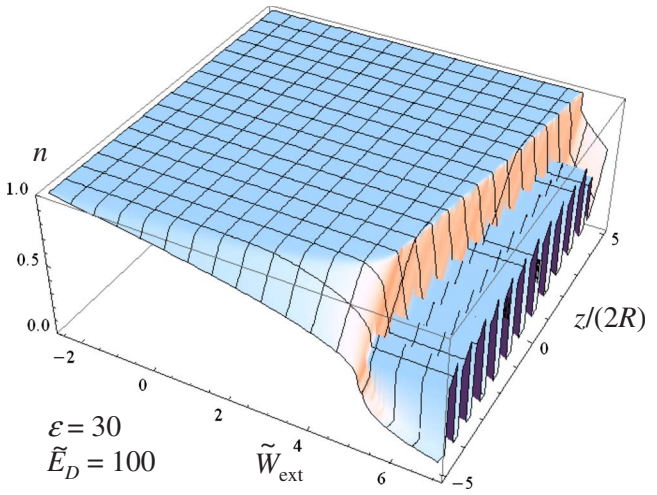

FIG. 8. (Color online) Wall of tunneling at $\tilde{E}_D=100$, ignited by slow sweep of the bias field, $\varepsilon=30$. The process starts at $\tilde{W}_{\rm ext}\approx 5$.

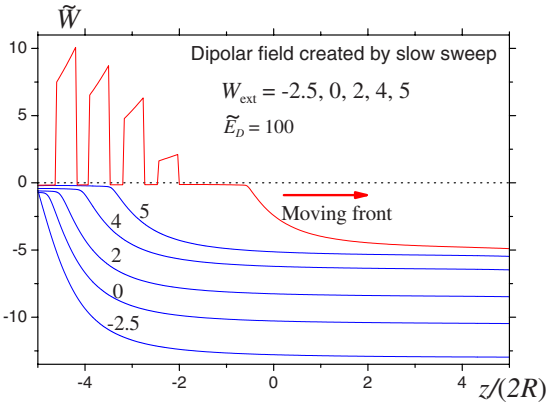

FIG. 9. (Color online) Dipolar field in the crystal at different values of $\tilde{W}_{\rm ext}$ during sweep. After $\tilde{W}_{\rm ext}=5$ the front starts moving and dipolar field in the sample becomes discontinuous.

the resonance. After some time the region close to the resonance becomes broad that is similar to the structure of the cold-deflagration front (see Fig. 9). In this way the initial state for the cold deflagration is being prepared. The front starts as the bias reaches the "magic" value of $\tilde{W}_{\rm ext}$ that weakly depends on $\tilde{E}_D$. For $\tilde{E}_D=20$ one has $\tilde{W}_{\rm ext}=4.3$ (that corresponds to $B_z-B_k\simeq 19$ mT) and for $\tilde{E}_D=100$ one has $\tilde{W}_{\rm ext}\simeq 5$. At such a strong bias there is a quasiperiodic spatial structure with discontinuous magnetization and the dipolar field behind the front, as shown in Figs. 8 and 9. One can see in Fig. 9 that in the moving front the bias is slightly below zero. This means that the system is somewhat off-resonance and this is the reason for a small front speed in this regime, as shown in Fig. 5.

The next question is how to ignite cold deflagration for arbitrary values of the external bias $\tilde{W}_{\rm ext}$ given by Eq. (30). The answer is to sweep B_z up to this value of $\tilde{W}_{\rm ext}$ and then to stop this (global) sweep at some $t_{\max,0}$. After that further sweep B_z locally near the end of the sample, $z=-L/2$, using a small coil. For the coil of radius R_0 placed at z_0 (the axis of the coil coincides with the axis of the cylinder) the local addition to $W_{\rm ext}$ can be written in the form

$$\delta W_{\rm ext}(z,t) = \frac{R_0^2}{R_0^2+(z-z_0)^2} v_W (t - t_{\max,0}) \qquad (56)$$

with $z_0\approx -L/2$. Numerical calculations with $R_0=R$ and $z_0=-L/2$ show that, indeed, with this method one can ignite fronts at different biases $\tilde{W}_{\rm ext}$, including the laminar regime (see Fig. 10). Here, the front is much faster than in Fig. 8, in accordance with the results for the front speed in Fig. 5(a). Total bias in the sample at different times is shown in Fig. 11. For instance, $\tau\equiv\Gamma_{\rm res}t=5000$ corresponds to the stage of the global sweep. All other times correspond to the local-sweep stage, since the bias curves converge on the right side of the sample where $\delta W_{\rm ext}$ is small. Local sweep near the left end creates an initial state for the front to start, as the bias curves are approaching zero in a progressively large region (blue curves). As the front starts moving (red curves), the bias becomes positive on the left with nonlaminar features near the end. But in the depth of the sample the front is laminar corresponding to $\tilde{W}_{\rm ext}=1$.

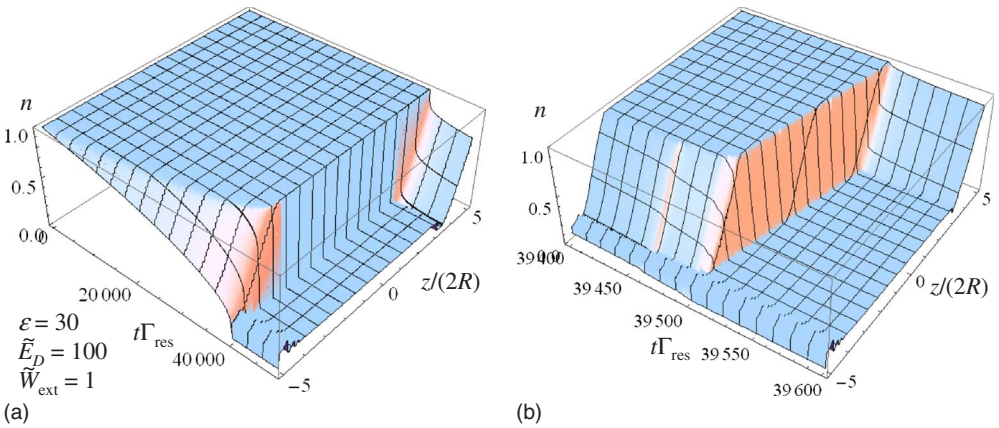

FIG. 10. (Color online) Laminar front of tunneling at $\tilde{E}_D=100$ and $\tilde{W}_{\rm ext}=1$ ignited by slow *local* sweep of the bias field. (a) Overview; (b) zoom of the front region.

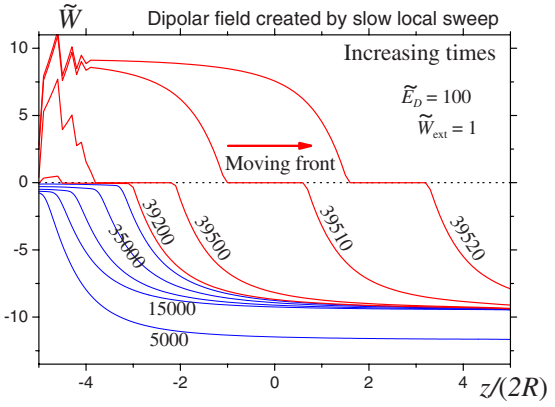

FIG. 11. (Color online) Total bias at different times in the laminar front of tunneling at $\tilde{E}_D=100$ and $\tilde{W}_{\rm ext}=1$ ignited by slow local sweep of the bias field. Blue lines correspond to times of adjustment before ignition and red lines correspond to the moving front.

VIII. DISCUSSION

In the main part of the paper it was shown that elongated crystals of molecular magnets (practically Mn_{12} Ac) can exhibit moving fronts of dissipative spin tunneling at biased resonances, Eq. (3) with $k>0$. This phenomenon is resembling magnetic deflagration,[20,21] only the relaxation rate is controlled by the dipolar field evolving self-consistently and bringing the spins in the front region on and off tunneling resonance, rather than by the temperature. Like deflagration, it leads to destruction of the initial metastable ordered state, this is why it can be called "cold deflagration." A signature of the cold deflagration is an incomplete transition from the metastable to stable state. In Ref. 18 it was argued that cold deflagration can be responsible for the experimentally observed steps in dynamic hysteresis loops.

Of course, transitions at biased resonances result in energy release and warming of the sample, so that the two mechanisms can coexist. In fact, magnetic deflagration was observed in crystals of Mn_{12} Ac thermally isolated so that the warming of the sample is efficient. Without thermal isolation, cold deflagration does not face this competition. To further reduce heating, it is preferable to work at low bias.

There are two regimes of cold deflagration: laminar regime at low-bias B_z-B_k and nonlaminar regime at high bias. In the laminar regime the magnetization in the front adjusts so that the dipolar-field $B^{(D)}$ together with the external-field B_z creates a nearly zero bias for the resonance transitions in the front region with the width of order R, the transverse size of the crystal. In the laminar regime the magnetization and dipolar field in the sample are continuous and both the front speed and the magnetization (metastable population) behind the front can be found analytically in the practical limit of the strong dipolar field, [Eqs. (53) and (41)]. Remarkably, both of these quantities do not depend on the strength of the dipolar-field E_D in this region.

In the laminar regime the estimation for the front speed is $v\sim R\Gamma_{\rm res}$, where $\Gamma_{\rm res}$ is the transition rate at resonance, $W=0$ in Eq. (12). At the boundary between the over- and underdamped regimes, $\Delta\sim\Gamma_{m'}$ and thus $\Gamma_{\rm res}\sim\Gamma_{m'}$ (that is realized in the transverse field 3 T in Mn_{12} Ac at the $k=1$ resonance) cold deflagration already beats the regular "hot" deflagration. Indeed, the latter has the speed $v\sim l\Gamma(T_f)$, where l depends on the thermal diffusivity but experimentally is comparable with R and $\Gamma(T_f)$ is the thermal activation rate over the barrier at the flame temperature. Since $\Gamma(T)$ at high temperatures is determined by the rates of transitions between adjacent levels near the top of the barrier that are smaller than the same for low-lying levels such as $\Gamma_{m'}$ (one has $\Gamma(T_f)\sim 10^6$ s^{-1} and $\Gamma_{S-1}\sim 10^7$ s^{-1}) the hot deflagration loses.

At higher-bias B_z-B_k the laminar regime breaks down, the dipolar field cannot fully adjust to provide a nearly zero bias in the front's core, and the magnetization and the dipolar field become discontinuous. There are frozen-in quasiperiodic spatial structures behind the front. Accordingly, the front speed dramatically drops (see Fig. 5), especially in the case of a strong dipolar field. There is no analytical solution in this range but the fit to the numerical results yields $v\propto 1/E_D^2$. The boundary between the laminar and nonlaminar regimes corresponds to $B_z-B_k=5-10$ mT.

It was shown that cold deflagration can be ignited by the local sweep of the field B_z near an end of the crystal. This local field can be produced by a small coil with increasing current.

Another condition for the observability of the cold deflagration is sufficiently strong transverse field that allows tunneling transitions via low-lying levels.

At nonzero temperatures the rate of cold deflagration should increase because of the activation to higher levels providing a higher transition probability [see Eq. (10) of Ref. 18].

Different kinds of disorder, such as solvent disorder, hyperfine fields from nuclear spins, etc., lead to the resonance condition for tunneling being different at each lattice site. Numerical calculations within the present simplified $1d$ model show that the metastable populations adjust in a way that the dipolar fields at different lattice sites within the cold-deflagration front compensate for the random component of the bias, so that the system is on resonance everywhere within the front (see Fig. 5 of Ref. 18). For spin-tunneling fronts induced by sweep, there is no significant dependence of the "magic" value of the external bias at which the front starts on the disorder.

ACKNOWLEDGMENTS

The author is indebted to E. M. Chudnovsky for many stimulating discussions. This work has been supported by the NSF (Grant No. DMR-0703639).

[1] T. Lis, Acta Crystallogr., Sect. B: Struct. Crystallogr. Cryst. Chem. **36**, 2042 (1980).
[2] A. C. R. Sessoli, D. Gatteschi, and M. A. Novak, Nature (London) **365**, 141 (1993).
[3] J. R. Friedman, M. P. Sarachik, J. Tejada, and R. Ziolo, Phys. Rev. Lett. **76**, 3830 (1996).
[4] J. M. Hernández, X. X. Zhang, F. Luis, J. Bartolomé, J. Tejada, and R. Ziolo, EPL **35**, 301 (1996).
[5] L. Thomas, F. Lionti, R. Ballou, D. Gatteschi, R. Sessoli, and B. Barbara, Nature (London) **383**, 145 (1996).
[6] A. Morello, F. L. Mettes, F. Luis, J. F. Fernández, J. Krzystek, G. Aromi, G. Christou, and L. J. de Jongh, Phys. Rev. Lett. **90**, 017206 (2003).
[7] D. A. Garanin and E. M. Chudnovsky, Phys. Rev. B **78**, 174425 (2008).
[8] S. McHugh, R. Jaafar, M. P. Sarachik, Y. Myasoedov, H. Shtrikman, E. Zeldov, R. Bagai, and G. Christou, Phys. Rev. B **79**, 052404 (2009).
[9] N. V. Prokof'ev and P. C. E. Stamp, Phys. Rev. Lett. **80**, 5794 (1998).
[10] A. Cuccoli, A. Fort, A. Rettori, E. Adam, and J. Villain, Eur. Phys. J. B **12**, 39 (1999).
[11] J. J. Alonso and J. F. Fernández, Phys. Rev. Lett. **87**, 097205 (2001).
[12] J. F. Fernández and J. J. Alonso, Phys. Rev. Lett. **91**, 047202 (2003).
[13] P. C. E. Stamp and I. S. Tupitsyn, Phys. Rev. B **69**, 014401 (2004).
[14] I. S. Tupitsyn, P. C. E. Stamp, and N. V. Prokof'ev, Phys. Rev. B **69**, 132406 (2004).
[15] J. F. Fernández and J. J. Alonso, Phys. Rev. B **69**, 024411 (2004).
[16] J. F. Fernández and J. J. Alonso, Phys. Rev. B **72**, 094431 (2005).
[17] W. Wernsdorfer, T. Ohm, C. Sangregorio, R. Sessoli, D. Mailly, and C. Paulsen, Phys. Rev. Lett. **82**, 3903 (1999).
[18] D. A. Garanin and E. M. Chudnovsky, Phys. Rev. Lett. **102**, 097206 (2009).
[19] N. Avraham, A. Stern, Y. Suzuki, K. M. Mertes, M. P. Sarachik, E. Zeldov, Y. Myasoedov, H. Shtrikman, E. M. Rumberger, D. N. Hendrikson, N. E. Chakov, and G. Christou, Phys. Rev. B **72**, 144428 (2005).
[20] Y. Suzuki, M. P. Sarachik, E. M. Chudnovsky, S. McHugh, R. Gonzalez-Rubio, N. Avraham, Y. Myasoedov, E. Zeldov, H. Shtrikman, N. E. Chakov, and G. Christou, Phys. Rev. Lett. **95**, 147201 (2005).
[21] D. A. Garanin and E. M. Chudnovsky, Phys. Rev. B **76**, 054410 (2007).
[22] D. A. Garanin and E. M. Chudnovsky, Phys. Rev. B **56**, 11102 (1997).
[23] D. Garanin, arXiv:0805.0391 (unpublished).
[24] E. M. Chudnovsky, D. A. Garanin, and R. Schilling, Phys. Rev. B **72**, 094426 (2005).